Supplementary information

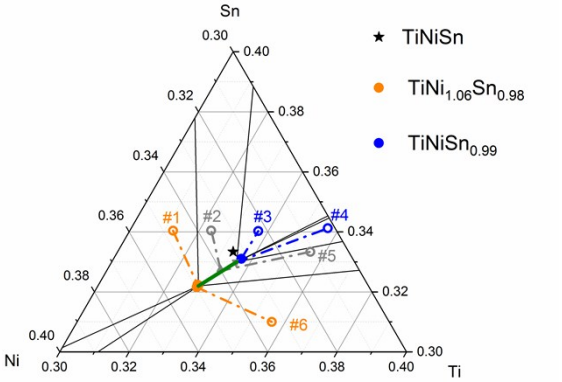

Figure S1. Magnification of phase regions near TiNiSn of isothermal section at 1223 K of Ti-Ni-Sn ternary phase diagram. The solid green line represents the single phase TiNiSn. The nominal sample compositions are shown as open circles. Solid symbols represent the composition of the TiNiSn majority phase according to the EPMA-WDS analysis for each element. The nominal (open circles) and experimental compositions (solid symbols) are connected with a dotted line.

(a) #1 $Ti_{31.3}Ni_{34.7}Sn_{34.0}$
Phase region: TiNiSn, $TiNi_2Sn$, and liquid Sn

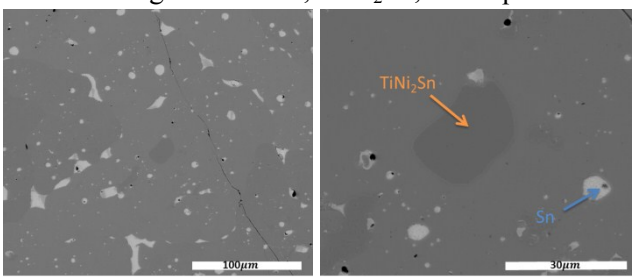

(b) #2 $Ti_{32.3}Ni_{33.6}Sn_{34.0}$
Phase region: TiNiSn and liquid Sn

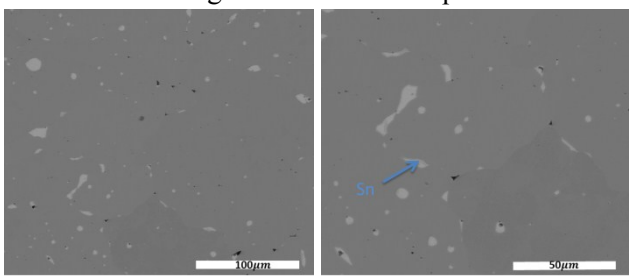

(c) #3 $Ti_{33.7}Ni_{32.3}Sn_{34.0}$
Phase region: TiNiSn, Ti_6Sn_5, and liquid Sn

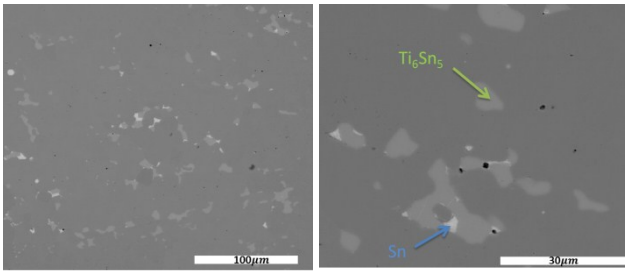

(d) #4 $Ti_{35.7}Ni_{30.2}Sn_{34.1}$
Phase region: TiNiSn, Ti_6Sn_5, and Ti_5NiSn_3

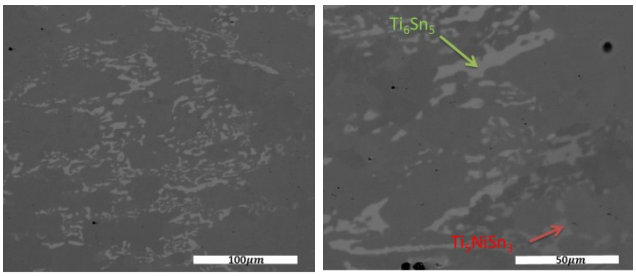

(e) #5 $Ti_{35.6}Ni_{31.1}Sn_{33.3}$
Phase region: TiNiSn and Ti_5NiSn_3

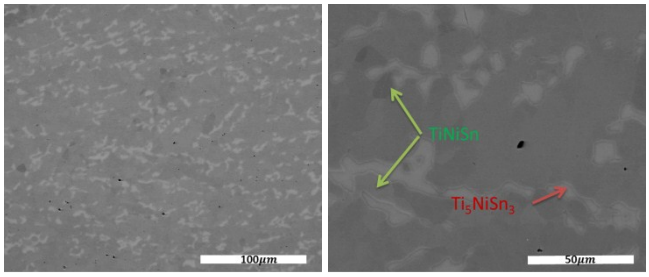

(f) #6 $Ti_{35.6}Ni_{33.4}Sn_{31.0}$
Phase region: TiNiSn, $TiNi_2Sn$, and Ti_5NiSn_3

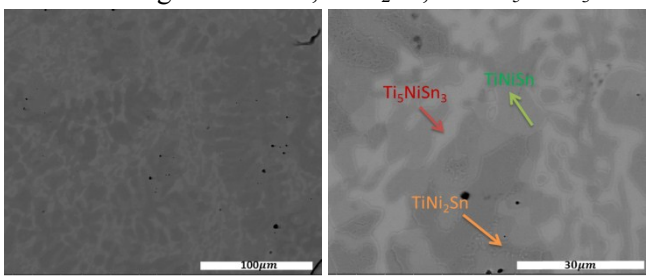

Figure S2. Backscatter electrons SEM images of TiNiSn with different compositions annealed at 1223 K. Black regions are voids formed by thermal contraction during quenching.

Table S1. Actual composition of TiNiSn phases with different nominal compositions for phase diagram study according to EPMA-WDS analysis carried out on the Half-Heusler phase region.

Nominal composition	Annealing T(K)	EPMA-WDS composition
#1 $Ti_{31.3}Ni_{34.7}Sn_{34.0}$	923	$Ti_{33.3(4)}Ni_{33.4(3)}Sn_{33.2(3)}$
	1073	$Ti_{33.3(2)}Ni_{34.0(1)}Sn_{32.7(1)}$
	1223	$Ti_{32.9(2)}Ni_{34.9(1)}Sn_{32.2(1)}$
#2 $Ti_{32.3}Ni_{33.6}Sn_{34.0}$	1223	$Ti_{33.3(1)}Ni_{34.0(1)}Sn_{32.8(1)}$
#3 $Ti_{33.7}Ni_{32.3}Sn_{34.0}$	1073	$Ti_{33.6(1)}Ni_{33.1(2)}Sn_{33.2(1)}$
	1223	$Ti_{33.5(2)}Ni_{33.2(1)}Sn_{33.3(1)}$
#4 $Ti_{35.7}Ni_{30.2}Sn_{34.1}$	1223	$Ti_{33.4(1)}Ni_{33.4(2)}Sn_{33.2(1)}$
#5 $Ti_{35.6}Ni_{31.1}Sn_{33.3}$	1223	$Ti_{33.2(1)}Ni_{34.1(2)}Sn_{32.7(1)}$

#6 $Ti_{35.6}Ni_{33.4}Sn_{31.0}$	1223	$Ti_{32.8(2)}Ni_{35.0(3)}Sn_{32.2(3)}$

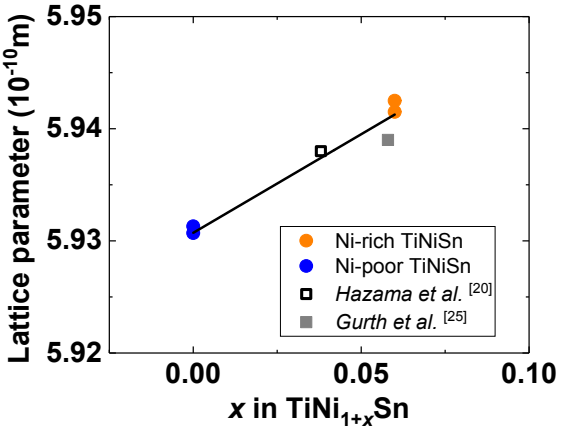

Figure S3. Lattice parameter derived from XRD analysis of the TiNiSn Half-Heuslers annealed at 1223 K. Blue ones are for Ni-poor samples; orange symbols are for Ni-rich samples. *x* indicates the excess Ni content in $TiNi_{1+x}Sn$. Grey and black symbols are from literature.[1,2]

Table S2. Transport properties at 500 and 700 K of Ni-rich and Ni-poor TiNiSn Half-Heuslers as a function of Sb doping quantified by the variable *x* determined by EPMA-WDS analysis.

T=500K

Stable boundary compositions	EPMA Sb *x*	n_H (cm^{-3})	Seebeck (μVK^{-1})	Mobility ($cm^2V^{-1}s^{-1}$)	Conductivity ($10^5S/m$)	κ_l ($Wm^{-1}K^{-1}$)	zT
Ni rich $TiNi_{1.06}Sn_{0.98-x}Sb_x$	**0**	2.2E+20	-197.9	15.5	0.66	3.04	0.36
	0.013 ± 0.003	4.6E+20	-140.0	16.1	1.49	2.80	0.35
	0.003 ± 0.000	2.2E+20	-170.8	14.7	0.77	2.79	0.33
	0.017 ± 0.003	4.4E+20	-151.8	17.6	1.22	2.83	0.36
Ni poor $TiNiSn_{0.99-x}Sb_x$	**0**	1.4E+20	-212.9	20.0	0.44	4.16	0.22
	0.011 ± 0.003	3.5E+20	-157.4	21.3	1.30	4.10	0.31
	0.020 ± 0.006	6.5E+20	-128.8	18.3	2.04	4.07	0.28
	0.055 ± 0.006	1.4E+21	-81.1	16.0	3.69	4.15	0.15

T=700K

Stable boundary compositions	EPMA Sb *x*	n_H (cm^{-3})	Seebeck (μVK^{-1})	Mobility ($cm^2V^{-1}s^{-1}$)	Conductivity ($10^5S/m$)	κ_l ($Wm^{-1}K^{-1}$)	zT
Ni rich $TiNi_{1.06}Sn_{0.98-x}Sb_x$	**0.013 ± 0.003**	5.0E+20	-152.6	13.5	1.47	2.62	0.54
	0.017 ± 0.00	5.6E+20	-163.7	13.7	1.23	2.53	0.57

	3						
Ni poor	**0.020 ± 0.006**	7.0E+20	-153.0	13.4	1.63	3.27	0.50
$TiNiSn_{0.99-x}Sb_x$	**0.055 ± 0.006**	1.2E+21	-107.0	14.3	2.74	3.15	0.32

Band modeling

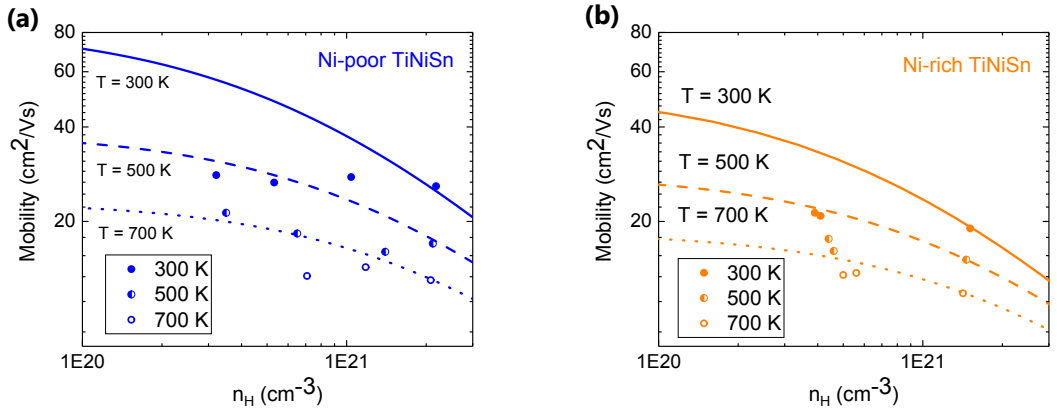

Figure S4: Mobility as a function of Hall carrier concentration n_H at different temperatures for (a) Ni-poor TiNiSn and (b) Ni-rich TiNiSn. In (a), the lines represent the mobility calculated assuming acoustic phonon scattering only with E_{def} = 5.2 eV. In (b), the lines represent the mobility calculated including in addition alloy scattering due to excess Ni with E_{alloy} = 0.5 eV. All data points are from high temperature Hall measurements at temperature below the onset of thermal excitations of carrier across the band gap.

A single Kane band model is used with a density-of-states effective mass of 2.8 m_e. An experimental band gap of 0.26 eV and band anisotropy parameter of 5.2 from literature is chosen [3]. Figure S4 shows the mobility Pisarenko trend for the Ni-rich and Ni-poor samples. Polar optical phonon scattering contributes mainly at low carrier density and can thus be neglected at high carrier density.[4,5] Alloy scattering due to Sb doping is neglected here due to the similar size and mass of Sn and Sb. Assuming only acoustic phonon scattering for the Ni-poor sample, the deformation potential for acoustic phonon scattering can be estimated. Employing a temperature independent deformation potential E_{def}, a value of 5.2 eV is extracted from the three data points at 2.2E21cm^{-3} in Fig. S4a. The mobility at lower carrier density deviates to lower values due to polar optical phonon scattering. For the Ni-rich sample, alloy scattering plays an important role in addition to acoustic phonon scattering, as discussed in conjunction with Fig. 3b. Employing a temperature independent deformation potential of 5.2 eV, assumed to be identical as for the Ni-poor case, an alloy scattering potential E_{alloy} of 0.5 eV is extracted from the three data points at 1.5E21cm^{-3} in Fig. S4b. Also for the Ni-rich sample, the mobility observed at lower carrier density deviates to lower values due to polar optical phonon scattering.These extracted values (E_{def} = 5.2 eV, E_{alloy} = 0.5 eV) are close to those of ZrNiSn (E_{def} = 5eV, E_{alloy} = 0.9 eV)[5]. Yet they serve only as a rough estimate. In order to get rigorous values, a more detailed investigation is necessary.

Electron probe micro-analyses

The carbon coated (20 nm) polished Half – Heusler samples were analysed with a Jeol JXA-8200 electron probe microanalyser (EPMA), using wavelength dispersive X-ray spectrometry (WDS). Operation conditions were 17 kV, 20 and 30nA using a focussed electron beam. In the first part of the study, samples were analysed for Sn, Ti and Ni, using the K_α line for Ni and Ti and the L_α line for Sn. Background and appropriate monochromator crystals were determined by means of qualitative WDS-scans on the samples (Sn, PETJ: +3.5 / -3.5 mm; Ti, PETJ: +5 / -2 mm; Ni, LIFH: +3.5 / -3.5 mm). In the course of the study, Sb was added to the metal alloys, which was analysed using the Sb L_α line. Due to the interference of the Sn L_β peak with the lower angle background of the Sb L_α peak, only one background could be analysed (Sb, PETH, +1.5 / 0). Analysing the lower background behind the Sn L_β peak was considered not to be suitable due to a second diffraction order of Ni at lower angle of the Sn L_β peak, which could not be fully supressed by means of the energy discriminator of the single channel analyser. Standards used were ultrapure metals of the single elements from Alfa Aesar. Peaks and background were analysed during 30 seconds each and energy discriminators were employed for all elements to reduce higher order diffractions. Results were processed using the quantitative inter-element matrix correction procedures $\phi(\rho z)$ (Armstrong , 1988) as implemented in the EPMA software, which is correcting for the stopping power, backscatter coefficient, absorption and fluorescence.[6] Provided errors are absolute 2σ errors, based on the Poisson counting statistics of the standard and the individual analyses.

1 Gürth, M. *et al.* On the constitution and thermodynamic modelling of the system Ti–Ni–Sn. *RSC Adv.* **5**, 92270-92291, doi:10.1039/c5ra16074j (2015).

2 Hazama, H., Matsubara, M., Asahi, R. & Takeuchi, T. Improvement of thermoelectric properties for half-Heusler TiNiSn by interstitial Ni defects. *Journal of Applied Physics* **110**, 063710, doi:10.1063/1.3633518 (2011).

3 Komar, P. *et al.* Tailoring of the electrical and thermal properties using ultra-short period non-symmetric superlattices Supplemental Material. *APL Materials* **4**, 104902 (2016).

4 Wang, H., Pei, Y., LaLonde, A. D. & Jeffery Snyder, G. in *Thermoelectrics Nanomaterials* Vol. 182 (eds K. Koumoto & T. Mori) 3-32 (Springer, 2013).

5 Xie, H. *et al.* Beneficial Contribution of Alloy Disorder to Electron and Phonon Transport in Half-Heusler Thermoelectric Materials. *Advanced Functional Materials* **23**, 5123-5130, doi:10.1002/adfm.201300663 (2013).

6 Armstrong, J. T. in *Microbeam Analysis* (ed D. E. Newbury) 239-246 (San Francisco Press Inc., 1988).